The effect of residual stress on mixed-mode crack propagation behavior in friction stir welded 7075-T6 aluminum alloy panel under biaxial loading

Xiushuo Zhang[1], Yu E Ma[1], Zhenhai Wang[2], Yanning Guo[1]

[1]School of Aeronautics, Northwestern Polytechnical University, Xi'an, 710072, China
[2]School of Mathmatics and Statistics, Northwestern Polytechnical University, Xi'an, 710072, China

Correspondence
Y. Ma and Z. Wang, School of Aeronautics, Northwestern Polytechnical University, Xi'an, 710072, China; School of Mathmatics and Statistics, Northwestern Polytechnical University, Xi'an, 710072, China
Email: ma.yu.e@nwpu.edu.cn; zhwang@nwpu.edu.cn

Funding information
National Natural Science Foundation of China, Grant/Award Numbers:11572250, 91860128; 2018 Innovation Ability Supporting Program of ShaanXi Province, Grant/ Award Number: 2018KW-028

Abstract: In this work, the effect of residual stress on mixed-mode crack propagation behavior in friction stir welded (FSW) 7075-T6 panel under biaxial loading was investigated. The cruciform sample was designed and manufactured by FSW. Residual stress profiles across the welded sample were measured by the X-ray diffraction technique. Crack propagation behaviors were simulated with five different biaxial loading ratios. Stress intensity factors (K_I and K_{II}) were evaluated by finite element method (FEM) and used to study the effects of residual stress on crack behaviors. It was observed that residual stress has a considerable effect on the mixed-mode crack growth. In most of the cases, the crack deflection is mainly affected by residual stress at the beginning of crack propagation. The variation of crack propagation path is strongly linked with the residual stress as well as the biaxial loading ratio. In addition, K_I and K_{II} are susceptible to residual stress under biaxial loading conditions. Residual stresses contribute to a higher proportion of K_{II}

compared to that of K_I. K_I and K_{II} in the retreating side are more affected by the residual stress.

KEYWORDS : friction stir welding; residual stress; biaxial loading; mixed-mode fatigue crack propagation; crack path

NOMENCLATURE

a_0	half crack length for an initial crack
E	Young's modulus
FCGR	fatigue crack growth rate
FEM	finite element method
FSW	friction stir weld
G	energy release rate
IIM	interaction integral method
J	path-independent *J*-integral
J^{load}	*J*-integral for the actual field (applied load)
J^{res}	*J*-integral for the auxiliary field (residual stress)
$\overline{J}$	*J*-integral for the superimposed fields (actual and auxiliary)
K_I, K_{II}	mode I, II stress intensity factor
K_{eq}	equivalent stress intensity factor
K_{IC}	mode I fracture toughness
K_I^{load}, K_{II}^{load}	mode I, II stress intensity factor caused by the applied load
K_I^{res}, K_{II}^{res}	mode I, II residual stress intensity factor
$\triangle K_{th}$	threshold value of stress intensity factor range
M	interaction integral (M-integral)
n_j	outward normal vector; $j = 1,2$

P_x, P_y	applied load in the horizontal and vertical directions respectively
q	weight function in the domain integral
RS	residual stress
SIFs	stress intensity factors
$u_{i,j}^{(1)}$	displacement derivatives for the actual field (applied load); $i, j = 1,2$
$u_{i,j}^{(2)}$	displacement derivatives for the auxiliary field (residual stress); $i, j = 1,2$
W	strain energy density
WRS	welding residual stress
XRD	X-ray diffraction
α	inclination angle of oblique crack respect to horizontal axis
Γ	contour for *J* and *M* integrals
Γ_s	inner contour
δ_{ij}	Kronecker delt; $i, j = 1,2$
ε_{ij}	strains tensor; $i, j = 1,2$
θ	crack propagation angle
λ	biaxial loading ratio
σ_{ij}	stress tensor; $i, j = 1,2$

1 INTRODUCTION

In the past few decades, the design concepts for aircraft structures have been developed in order to enhance reliability, reduce part weight and saving costs. The conventional technologies, such as riveting and bolting, are difficult to meet the new demands. Friction stir welding (FSW) is being explored as a promising technology for aircraft construction where it can be used to substitute for mechanical fastening or riveting.[1] FSW is a solid-state joining technology patented by The Welding Institute

(TWI) of UK in 1991,[2] and it is applied to weld high-strength alloy for aeronautical structures. FSW has many advantages over other welding technologies in many ways, and it can be used to weld dissimilar metal materials, such as highly alloyed 2XXX and 7XXX series which are generally classified as non-weldable materials by the conventional fusion weld methods. Friction stir welding takes place at lower temperature level; thus, the magnitudes of residual stress (RS) are considerably lower than those measured in the fusion ones. These residual stresses arise mainly from the localized application of heat and rigid clamp restraint in FSW.[3,4]

In general, the presence of residual stress has an effect on the fatigue properties of the different weld zones in FSWed components.[5,6] John et al[7] investigated the relationship between residual stresses and fatigue crack growth rate (FCGR) in friction stir welded 7050-T7451. The FCGR in the heat affected zone (HAZ) is slower than in the base metal (BM). Pao et al[8] and Jata et al[9] studied residual stress and its effects on fatigue crack propagation in FSWed 7050-T7451. It is shown that the FCGR in the BM is higher than in the HAZ but lower than in the weld nugget (WN).

Some studies have shown that crack paths respond to mixed-mode stress field, this behavior is found in FSWs via changes in their trajectory. Pouget et al[6] studied fatigue crack path in FSWed AA2050 and performed fatigue tests under mode I condition. Because of residual stresses, the crack deviates from mode I into mixed-mode I/II both in the as-welded and post-weld heat treated conditions. Ma et al[10] investigated the fatigue crack paths in a FSWed 2198-T8 SE(T) plates with pad-up. The experimental and numerical simulation results show that welding residual stress (WRS) changes the crack turning point and the effective crack length. The crack changes from mode I to mixed-mode I/II when the crack deviates from the original path. However, those works are carried out under uniaxial loading condition. In practice, the load on aerospace components such as the fuselage skin are often biaxial. The concept of integral structure by the FSW technology is used in the fuselage panel. In the aircraft structure, a welded fuselage panel subjected to the combined action of longitudinal and transverse loading. If crack occurs in the weld nugget it will

propagates under the combination of biaxial loading and residual stress.

In order to study the crack propagation behavior under biaxial loading conditions, many researchers have done lots of works.[11-18] Misak et al[11,12] investigated the mixed-mode FCGR in cruciform specimens with a 45° inclined center notch under various mixed-mode biaxial loading conditions. They have reported that the FCGR in biaxial tension fatigue with higher biaxiality ratio is faster than that with lower biaxiality ratio at a given crack driving force level. But the opposite result is observed in the studies of mode I fatigue crack propagation. The reason is that the compressive stress parallel to the crack causes a decrease of crack growth rate.[13,14]

Some studies investigated the variation of crack propagation path in biaxial fatigue. Truchon et al[13] performed biaxial fracture tests of E36-Z steel with an initial transverse crack and observed an S-shaped crack propagation path in a biaxial stress field where $\sigma_x > \sigma_y$. Kibler et al[15] investigated biaxial fracture tests of 6061-T4 and 6061-T6 aluminum samples. The results show that the crack propagation path varies with the biaxial loading ratio. Lee et al[16] conducted fatigue tests of aluminum alloy 1100-H14 and 7075-T651 samples with a transverse or a 45° inclined center notch under biaxial loading. They concluded that the crack propagation path is dominated by the stress biaxiality and the crack angle with respect to the applied principal stress direction. Zhang X and Richter et al[17,18] studied the fatigue crack propagation behavior in FSWed AA2198-T8 Al-Li alloy with a transverse center notch under equi-biaxial loading. The experimental results show that crack propagation path is symmetric in the specimens with weld parallel to the material rolling direction. Unfortunately, a notable distinction between the experimental and predicted crack propagation paths are observed, because the residual stress is not considered in the prediction model.

Results from previous studies have demonstrated that the experimental crack propagation paths and fracture surfaces in FSW joints are sensitive to residual stress field.[5-10,17-19] In order to understand the fatigue behavior in FSWed fuselage panel deeply, it is necessary to study the effect of residual stress on the fatigue crack

propagation in FSWed structures under biaxial loading. However, few works have studied the effect of residual stress under mixed-mode loading condition. Therefore, in this work, welded cruciform sample was designed to investigate the fatigue crack propagation behavior under in-plane biaxial loading condition. X-ray diffraction (XRD) was chosen to measure the distribution of residual stress across the weld in FSWed 7075-T6 Al alloy sheet. The effect of residual stresses on the mixed-mode fatigue crack propagation under different biaxial loading ratios was investigated.

2 MATERIAL AND SAMPLE PREPARATION

2.286 mm thick 7075-T6 Al alloy sheet is selected. Chemical compositions of 7075-T6 Al alloy are listed in Table 1. The sample is welded by FSW-RL31-010 machine in our university. The steel pin is 2.1 mm long and the diameter of the shoulder is 10mm. The rotated speed and the welding speed are 800 rpm and 100 mm/ min respectively.

TABLE 1 Chemical components of 7075-T6 Al alloy（wt. %）

Material	Si	Fe	Cu	Mn	Mg	Cr	Zn	Ti	Al
Al 7075-T6	≤0.40	≤0.50	1.2~2.0	≤0.30	2.1~2.9	0.18~0.28	5.1~6.1	≤0.20	Bal

There are many samples designed to perform the mixed-mode testing.[20] Two kinds are popular among these samples: one is compact tension-shear sample; the other one is the cruciform sample. Compared with the compact tension-shear sample, the cruciform sample can provide the complete range of mode mixities from pure mode I to pure mode II and it has the largest uniform nominal stress distribution in working area. By changing both initial crack inclination angle and the biaxial loading ratio, different combinations of modes I and II can be achieved.[21] So, the welded cruciform type sample was designed in our work. The sample size and the welded sample are shown in Figure 1(a) and (b). As welded, the cruciform sample is machined to have the overall length and width of 320 mm including the grip areas of the loading arms shown in Figure 1(a). The working area located in the middle is 80

mm×80 mm and is displayed as a red dotted area. Each arm is 80 mm wide and 120 mm long. At the center of the plate, a $2a_0$ = 3mm long initial crack is inclined at an angle 45° to the weld line shown in Figure 1(b). The biaxial loading ratio and the corresponding load with the stress ratio R=0 is listed in Table 2. The cruciform sample under two mutually orthogonal loads, P_x and P_y are applied in the horizontal and vertical directions respectively. $\lambda = P_x / P_y$ is the biaxial loading ratio.

TABLE 2 Biaxial loading ratio and the corresponding load (R=0)

λ	0	0.5	1	1.5	2
P_x (kN)	0	4	8	12	16
P_y (kN)	8	8	8	8	8

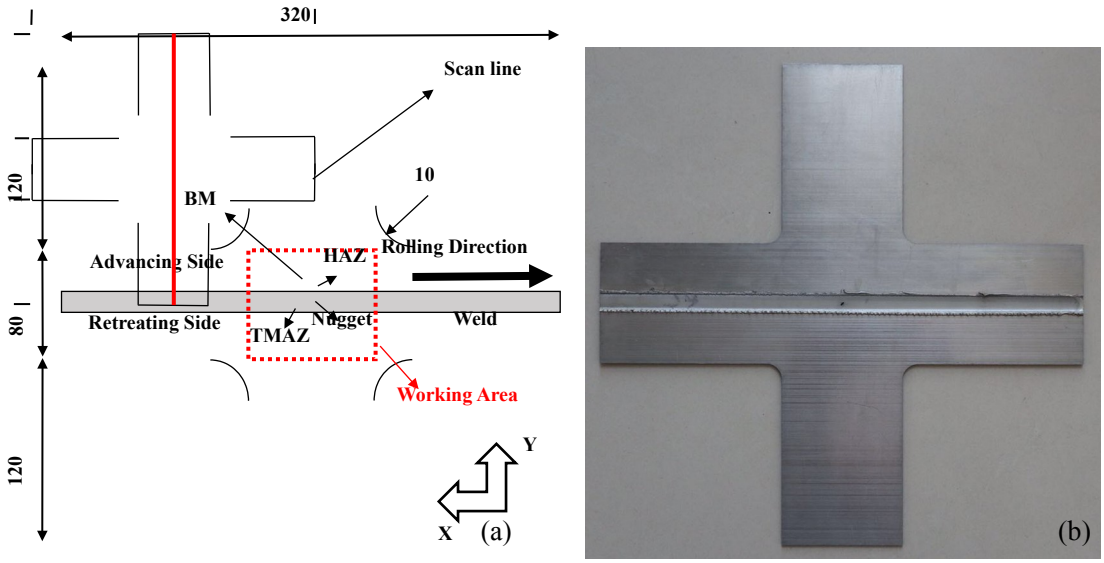

FIGURE 1 Cruciform sample for biaxial loading

(a) Sample size (b) Welded sample

3 RESIDUAL STRESS MEASUREMENT

Xstress Robot, an advanced X-ray stress analyzer, was used to measure residual stress in longitudinal and transverse directions shown in Figure 2. The voltage and the electrical current are 30 kV and 6.7 mA respectively. The detectors were set at a Bragg angle of 139.3° corresponding to diffraction at the (311) planes. The measurements were taken at 2θ scans from 131.7° to 146.3°, with 0.05° angle and 1s time increments per step, at five different tilt angles. Residual stresses were then computed by the $\sin^2\psi$ method.[22] Each point was repeated at least three times to evaluate the repeatability of data.

The scan line is placed perpendicular to the weld in the center of the sample shown in Figure 1. 23 measured points are set up along the scan line. The profile of residual stress is measured and shown in Figure 3. For longitudinal residual stress parallel to the direction of the weld. The distribution of residual stress presents a typical double-peaked shape around the weld. Residual stresses are tensile (8.5 ~ 43.6 MPa) in the weld zone and the heat affected zone in the vicinity of the weld (-10 ~ 15mm away from the weld). From the weld center to both sides, the tensile stress increases to two peak values. The maximum residual stress is 43.6 MPa at HAZ in the advancing side, while the maximal tensile stress in the retreating side is 35.3 MPa, 4mm away from the weld center. Then residual stresses decrease from tensile and turn to be compressive at 25mm. The maximum compressive residual stress is -50.2 MPa, 40 mm away from the weld center in the retreating side.

FIGURE 2 Xstress Robot

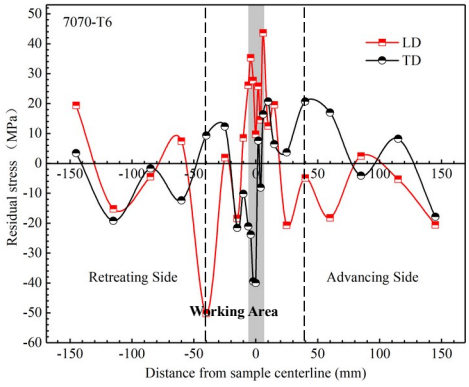

FIGURE 3 Residual stresses profile in FSW cruciform sample (LD and TD means longitudinal residual stress and transverse residual stress respectively)

For transverse residual stress normal to the direction of the weld, it shows a V-shaped in the working area. From the weld center to both sides, the maximal compressive residual stress is -40 MPa in the weld center. Residual stress remains compressive at the weld zone and the HAZ in the retreating side. Whereas, the residual stresses increase from compressive and turn to be tensile rapidly in the advancing side. The maximal values of tensile stress in the advancing side and the retreating side appear at 10 mm and -25 mm. Then tensile stress decreases and varies from 20.7 ~ -17.9MPa and 12.3 ~ -19.2MPa. Similar profiles have been measured by the neutron diffraction method in the published literatures.[23,24]

4 MIXED-MODE CRACK PROPAGATION MODELS

4.1 Analytical solution of stress intensity factor for cracks under biaxial loadings

For I/II mixed-mode cracks, the stress intensity factors (SIFs) can be calculated by Eq. (1) and Eq. (2).[25]

$$K_I = \sigma\sqrt{\pi a}\left(\lambda \sin^2\alpha + \cos^2\alpha\right) \quad (1)$$

$$K_{II} = \sigma\sqrt{\pi a}\left(1-\lambda\right)\sin\alpha\cos\alpha \quad (2)$$

where σ is the uniform extensional stress at infinity; α is the inclination angle of oblique crack to the horizontal axis; λ is the biaxial loading ratio.

4.2 Fatigue crack propagation models

At present, there are various fracture criteria to predict fatigue crack propagation

direction under mixed-mode loading. Erdogan and Sih[26] developed the maximum tangential stress criterion (MTS-criterion) which postulated that crack propagation will occur in the direction normal to the maximum tangential stress. Sih[27] presented the minimum strain energy density criterion (S-criterion) based on the concept of the strain-energy-density factor. The stationary values of this density factor can be used to predict the crack propagation direction under mixed-mode loading. Hellen et al[28] brought forward J-criterion, a path-independent line integrals, to study the problem of mixed-mode crack propagation. Theocaris et al[29,30] built the dilatational strain energy density criterion (T-criterion). The basic assumption is stated that a crack starts to propagate when the dilatational strain-energy at a point in the vicinity of its tip reaches a critical value. Li[31] introduced the vector crack tip displacement (CTD) criterion, and the vector crack tip displacement is used to describe the mixed-mode fatigue crack propagation. The tangential stress (strain) factor criteria proposed by Wu et al[32] postulated that the crack propagation occurs along the direction of the maximum tangential stress (strain) factor. Chambers et al[33] brought forward the criterion of maximum tangential strain, and this criterion can be used to investigate the direction of mixed-mode fatigue crack propagation under plane stress conditions. Among the established criterions, MTS-criterion has been widely used to study mixed-mode crack propagation due to its simplicity. According to this criterion, the mixed-mode crack propagation initiates radially from the crack tip along the direction ($\partial\sigma_{\theta,\max}/\partial\theta = 0$) in which the tangential stress reaches the maximum ($\sigma_{\theta\max}$). With the description of stress field near the crack tip under I/II mixed-mode loading, the crack extension direction can be found as

$$K_I \sin\theta + K_{II}\left(3\cos\theta - 1\right) = 0 \tag{3}$$

The solution of Eq. (3) can be expressed as

$$\theta = 2\tan^{-1}\left[\frac{1}{4\gamma} - \frac{1}{4}\sqrt{\left(\frac{1}{\gamma}\right)^2 + 8}\right], \quad K_{II} > 0$$

$$\theta = 2\tan^{-1}\left[\frac{1}{4\gamma}+\frac{1}{4}\sqrt{\left(\frac{1}{\gamma}\right)^{2}+8}\right],\ K_{II}<0\quad \gamma=\frac{K_{II}}{K_{I}} \tag{4}$$

In order to quantify the effect of the mixed-mode loading on the crack propagation, the concept of equivalent stress intensity factor (K_{eq}) is used for different types of mixed-mode fracture problems.[34] According to the energy balance criterion, the equivalent SIF can be derived as Eq. (5).[35]

$$K_{eq}=\sqrt{K_{I}^{2}+K_{II}^{2}} \tag{5}$$

Fatigue crack will propagates when the equivalent SIF reaches the threshold SIF, and the unstable fracture will take place if the equivalent SIF exceeds the fracture toughness,[36,37] as shown in Eq. (6). Mode I and mode II SIFs can be obtained as the crack grows. The fatigue crack propagation simulations are terminated when the equivalent SIF reaches the fracture toughness or the crack tip is out of the working area. The material properties are listed in Table 3. This analysis assumes that the elastic constant in weld area is 80% as much as that in base material due to the weakened mechanical properties in the weld zone.[38,39]

$$K_{eq} \quad K_{IC} \tag{6}$$

TABLE 3 The material properties of 7075-T6 Al alloy sheet[40,41]

Material	E (GPa)	ν	$\triangle K_{th}$ (MPa·m$^{1/2}$)	K_{IC} (MPa·m$^{1/2}$)
Al 7075-T6	71.7	0.33	1.3007	25

5.FATIGUE CRACK PROPAGATION SIMULATIONS

5.1 Fatigue crack propagation analysis

ABAQUS is used to build the finite element model and to perform finite element analysis. The crack propagation direction is predicted by MTS criterion according to Eq. (3) and Eq. (4). The flowchart of fatigue crack propagation analysis is shown in Figure 4. The mesh detail of the FE model is shown in Figure 5. The element size near

the crack tips is 0.15 mm. C3D8R elements are used and the total element is 45093. The measured residual stress is input in the finite element model by SIGINI subroutine. A static procedure in ABAQUS was used to calculate the equilibrium self-balanced stress state. And then, a crack was inserted in the FE model. As the crack grew, SIFs were calculated by the interaction integral method. This method is proved to be useful in structure analysis.[42-44]

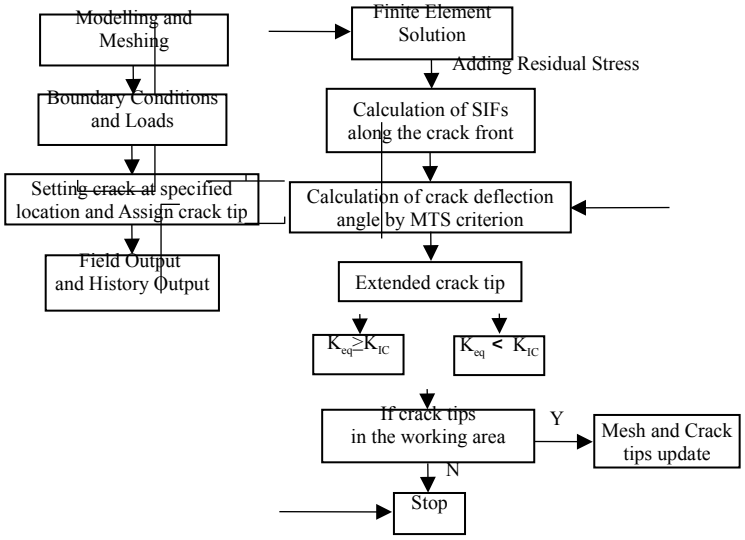

FIGURE 4 Flowchart of fatigue crack propagation analysis

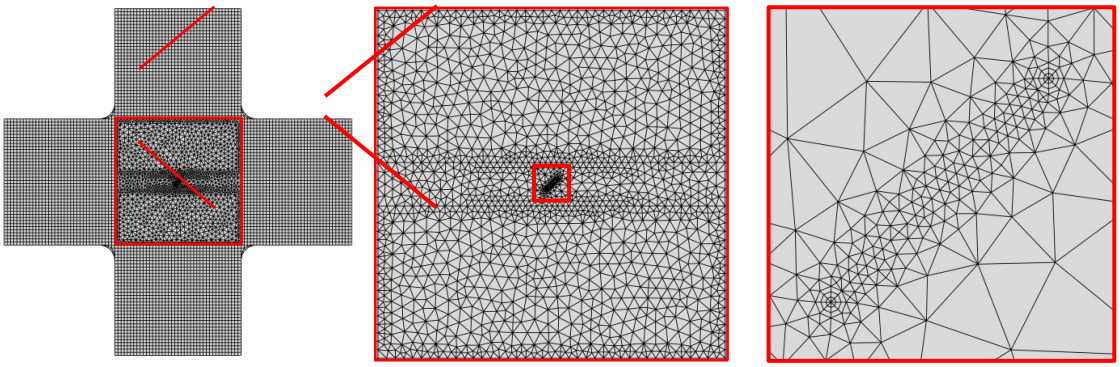

(a) (b) (c)

FIGURE 5 Finite element meshes used for the numerical simulation of cruciform sample

Mesh detail (a) in finite element model (b) in working area (c) around the crack tip

5.2 Evaluation of stress intensity factors

In the present work, the sample is only 2.286mm thin and it is under in-plane biaxial loading. Thus, the effect of through-the-thickness SIFs on the crack

propagation behavior can be neglected. Mode I and mode II SIFs under plane stress condition were evaluated by interaction integral method (IIM). This method was considered as the most readily and accurate technique to calculate the individual stress intensity factors for a crack under mixed-mode loading.[43,45]

The standard J-integral[46] is given by:

$$J = \lim_{\Gamma_s \to 0} \int_{\Gamma_s} \left(W\delta_{1j} - \sigma_{ij} u_{i,1} \right) n_j d\Gamma \tag{7}$$

where n_j is the outward normal vector to the contour Γ_s around the crack tip. W is the strain energy density given by Eq. (8):

$$W = \frac{1}{2}\sigma_{ij}\varepsilon_{ij} \tag{8}$$

J-integral can be written in domain integral method:

$$J = \int_A \left(\sigma_{ij} u_{i,1} - W\delta_{1j} \right) q_{,j} dA + \int_A \left(\sigma_{ij} u_{i,1} - W\delta_{1j} \right)_{,j} q dA \tag{9}$$

where q is a weight function. The J-integral of the superimposed fields (actual and auxiliary) is obtained as

$$\bar{J} = \int_\Gamma \left(\sigma_{ij}^{(1)} u_{i,1}^{(1)} + \sigma_{ij}^{(1)} u_{i,1}^{(2)} + \sigma_{ij}^{(2)} u_{i,1}^{(1)} + \sigma_{ij}^{(2)} u_{i,1}^{(2)} - W^{(1)}\delta_{1j} - W^{(2)}\delta_{1j} - W^{(1,2)}\delta_{1j} \right) q_{,j} ds \tag{10}$$

where $W^{(1,2)} = \sigma_{ij}^{(1)} \varepsilon_{ij}^{(2)} = \sigma_{ij}^{(2)} \varepsilon_{ij}^{(1)}$, superscript (1) and (2) correspond to the field variables in terms of the applied load and residual stress. In Eq. (10), $\bar{J}$ can be decomposed into three parts.

$$\bar{J} = J^{load} + J^{res} + M \tag{11}$$

$$\bar{J} = G_1 + G_2 = \frac{K_I^2 + K_{II}^2}{E} = \frac{1}{E}\left[\left(K_I^{load} + K_I^{res} \right)^2 + \left(K_{II}^{load} + K_{II}^{res} \right)^2 \right] \tag{12}$$

In this paper, $\bar{J}$ is obtained by superposition of the stress field and the auxiliary field near the crack tip.[47,48] G_1 and G_2 is the energy release rate which is related to the mixed-mode SIF. The auxiliary field (u^{res}, σ^{res}, ε^{res}) is residual stress field. K_I^{load},

K_{II}^{load}, K_{I}^{res} and K_{II}^{res} are the SIFs of mode I and mode II that caused by the applied load and residual stress. M is calculated by Eq. (13) and Eq. (14).

$$M=\int_{\Gamma}\left(\sigma_{ij}^{(1)}u_{i,1}^{(2)}+\sigma_{ij}^{(2)}u_{i,1}^{(1)}-W^{(1,2)}\delta_{1j}\right)q_{,j}ds \tag{13}$$

$$M=M^{(1)}+M^{(2)}=\frac{2}{E}\left(K_{I}^{load}K_{I}^{res}+K_{II}^{load}K_{II}^{res}\right) \tag{14}$$

K_{I}^{load} and K_{II}^{load} are evaluated as follows:

$$\left(K_{I}^{res}=1.0\ ,\ K_{II}^{res}=0.0\right),\ K_{I}^{load}=\frac{E}{2}M^{(1)} \tag{15}$$

$$\left(K_{I}^{res}=0.0\ ,\ K_{II}^{res}=1.0\right),\ K_{II}^{load}=\frac{E}{2}M^{(2)} \tag{16}$$

Then K_{I}^{res} and K_{II}^{res} can be determined.

5.3 Fatigue crack propagation path

The fatigue crack paths with and without residual stress for five biaxial loading ratios are shown in Figure 6. The crack tips close to the advancing side and the retreating side are defined as “front 1” and “front 2” respectively. The crack paths without residual stress (the solid line in Figure 6) agree with the experimental results (as the blue arrow shows). The initial crack deviation angle for different biaxial loading ratios are shown in Table 4.

For λ = 0, the crack path without residual stress is transverse shown in Figure 6 (a). For uniaxial λ = 0 test, the crack propagates at 90° to the resultant force, parallel to the *x*-axis.[49] For the case with residual stress under λ = 0 loading, crack grows almost straight after kinking and enter the base material at about ± 25mm. The crack path without residual stress deviates from the horizontal direction slightly with λ = 0.5, as indicated in Figure 6(b). The numerical result of the initial crack deviation angle under λ = 0.5 (38.9° in Table 4) is close to the experimental result, about 35° clockwise to the diagonal.[50] For the case of λ = 0.5 with residual stress, an S-shaped crack path is observed. The crack path seems to be significant affected by the residual

stress and immediately changes its main direction.

In Figure 6(c), the predicted result is validated by test data in biaxial tests under $\lambda = 1$ case without residual stress, the crack propagation path is diagonal along the 45° inclined notch.[50] For $\lambda = 1$ case with residual stress, crack path is similar to that without residual stress under $\lambda = 1.5$, as plotted in Figure 6(d). The reason is that the longitudinal and transverse residual stresses are added to the applied stresses, then the actual biaxial loading ratio is close to 1.5. For $\lambda = 1.5$ case without residual stress, the numerical initial crack deviation angle (27.8° in Table 4) approaches to the test values 29° counter-clockwise with the diagonal in the biaxial test,[51] as noted in Figure 6(d). For the case with residual stress under $\lambda = 1.5$ loading, the crack deviation angle increased to 35.1° and 36.5°.

In Figure 6(e), the crack propagation path without residual stress is vertical under $\lambda = 2$ loading. The predicted initial crack deviation angle (38.9° in Table 4) is close to the experimental result, about 34° counter-clockwise to the diagonal.[50] For $\lambda = 2$ with residual stress, the crack deviation angle is increased to 41.1° and 43.4°. Both the numerical and experimental crack propagation paths deflect to vertical direction for $\lambda = 1.5$ and 2.

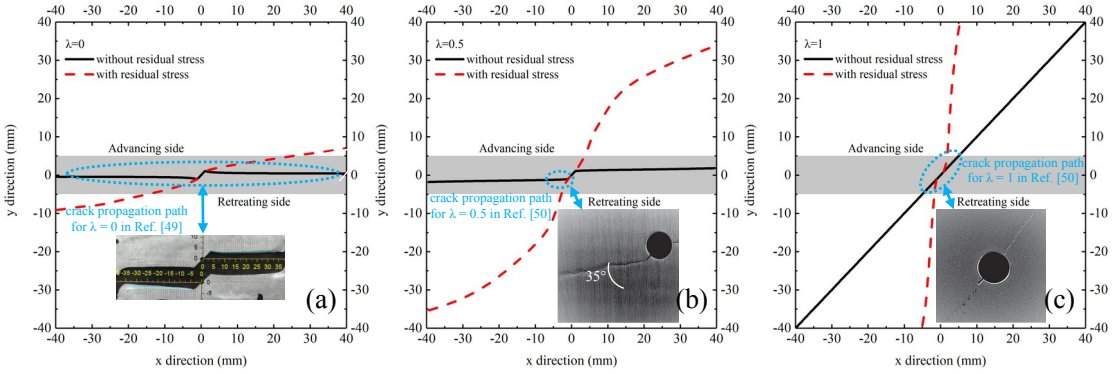

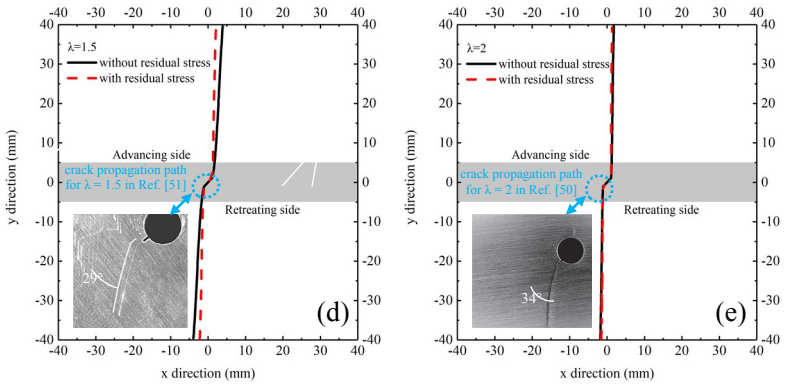

FIGURE 6 Crack propagation path in working area

(a) λ = 0 (b) λ = 0.5 (c) λ = 1 (d) λ = 1.5 (e) λ = 2

From the results illustrated in Figure 6, distinct differences are noticed for λ = 0, 0.5 and 1. Crack propagation paths are significantly affected by the residual stress field. Nevertheless, the effect of residual stress is decreased by the increased transverse load for λ = 1.5 and 2. To sum up, it reveals that residual stress is the main cause of a major loss of directional stability for λ = 0 ~ 1, but it has less effect on λ = 1.5 ~ 2.

TABLE 4 Initial crack deviation angle with respect to diagonal

λ	without residual stress	with residual stress-front 1	with residual stress-front 2
0	57.8° (clockwise)	26.1° (clockwise)	18.9° (clockwise)
0.5	38.9° (clockwise)	3.2° (counter-clockwise)	9.4° (counter-clockwise)
1	0°	24.3° (counter-clockwise)	27.2° (counter-clockwise)
1.5	27.8° (counter-clockwise)	35.1° (counter-clockwise)	36.5° (counter-clockwise)
2	38.9° (counter-clockwise)	41.1° (counter-clockwise)	43.4° (counter-clockwise)

The predicted crack deviation angles versus the crack length are plotted in Figure 7. For all studied cases without residual stress, the crack changes its direction at the beginning of crack propagation, and then grows straight (the crack deviation angle is 0° for λ = 1). In Figure 7(a) and (c)-(e), crack deviation angle changes obviously in

the early stage and fluctuates slightly with further crack growing for λ = 0, 1, 1.5 and 2 cases with residual stress. As shown in Figure 7(b), the crack angle changes continuously and shows significant deviations from its original direction on both sides with residual stress under λ = 0.5.

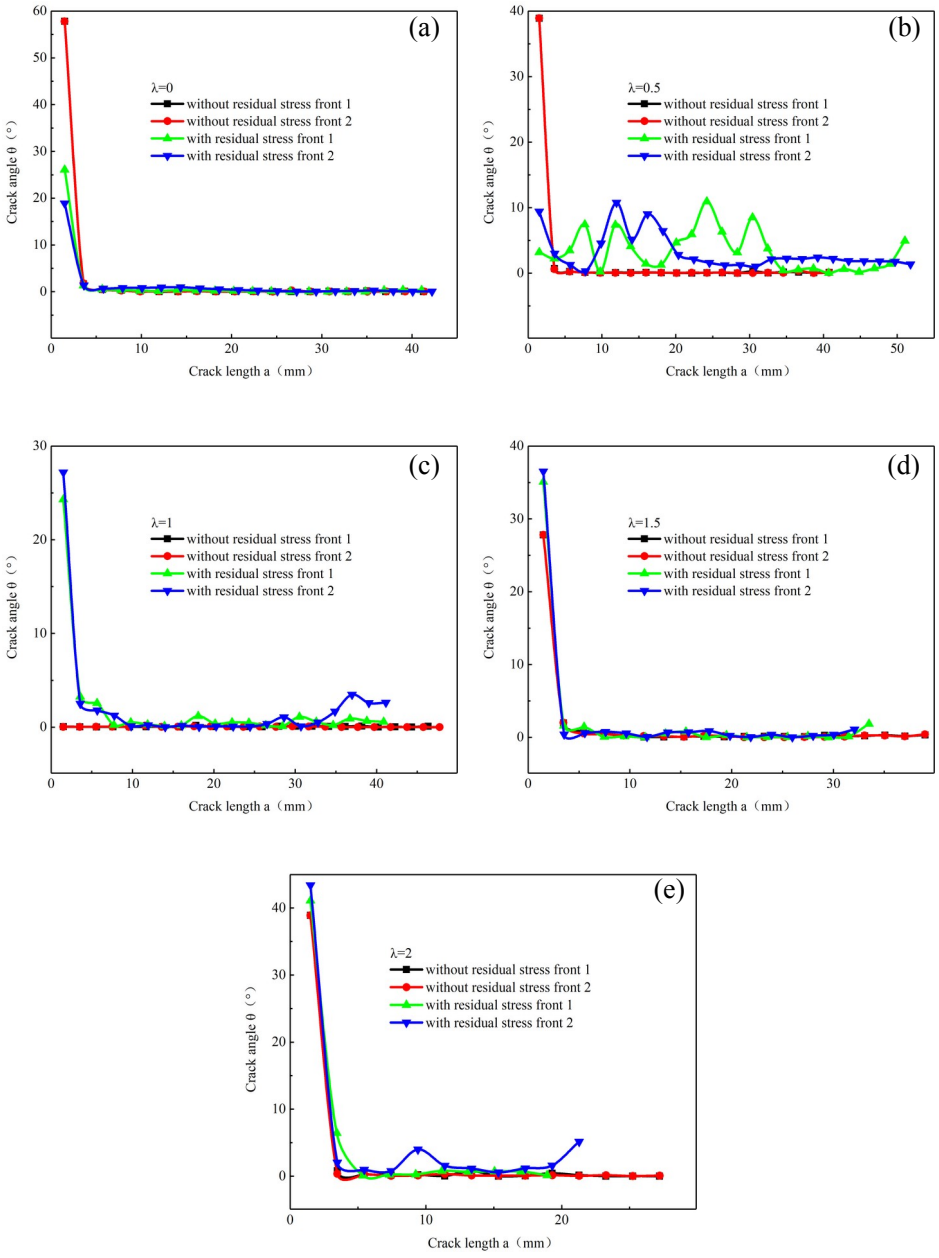

FIGURE 7 Crack deviation angle

(a) λ = 0 (b) λ = 0.5 (c) λ = 1 (d) λ = 1.5 (e) λ = 2

For λ = 0~2, the intersection angles between initial crack deflection with and without residual stress are calculated. The intersection angle of front 1 is 31.7°, 42.1°,

24.3°, 7.3° and 2.2°, and that of front 2 is 38.9°, 48.3°, 27.2°, 8.7° and 4.5°. It can be clearly observed that the effect of residual stress on the initial crack deflection increased from λ = 0 to λ = 0.5, and then decreased when λ >0.5. The asymmetrical distribution of residual stress reflects the discrepancy of crack propagation behavior between the advancing side and the retreating side. For example, in the case of λ = 0.5 with residual stress, the initial inclination angle of the oblique crack respect to diagonal along the 45° inclined crack on either side is 3.2° and 9.4°.

The initial crack angle changes and the cracks grow into the base material when residual stress profiles are input to the finite element models with λ = 0 and 0.5. For λ = 1, the crack propagation path which deflects to vertical direction is similar to the crack propagation path without residual stress for λ = 1.5. This indicates that the residual stresses caused the actual biaxial loading ratio higher than 1, and the nominal biaxial loading ratio is replaced by the actual biaxial loading ratio. Similar results have also been observed in Ref. [17]. In both cases (with and without residual stress), the crack propagation paths deflect to the vertical direction for λ = 1.5, and the intersection angle is within 8.7°. The effect of residual stress on initial crack angle is further reduced for λ = 2, and the difference between these two cases is within 4.5°. For λ = 0, 1, 1.5 and 2, the variation of crack deviation angle occurs mainly at the beginning of crack propagation. For λ = 0.5, the crack deviation angle changes continuously. In sum, residual stress has an important effect on the crack propagation for λ = 0.5, followed by λ = 1 and then λ = 0. A minor effect of residual stresses on the crack deviation angle is observed for λ = 1.5 and 2. The main reason is that the effect of residual stress on the crack propagation path is decreased with the increasing biaxial loading ratio.

5.4 K_I and K_{II} along crack path

K_I and K_{II} versus crack length for different biaxial loading ratios with and without residual stress on both sides are shown in Figure 8. For all studied cases without residual stress, K_I and K_{II} are the same on both sides of the crack at the

given biaxial loading ratio. K_I increases with the crack length. K_{II} decreases to zero as crack kinking (K_{II} is always zero for λ = 1), and crack grows straight.[52,53]

For all studied cases with residual stress, K_I induced by the combined effects of the applied load and the residual stress field is increased as the crack propagating. The presence of residual stress field leads to higher K_I at the initial crack tip, as illustrated in Figure 8(a), (c), (e), (g) and (i). In Figure 8(a), K_I at front 1 is quite close to that at front 2. As seen in Figure 8(c), K_I at front 1 is higher than that at front 2 when the crack length is 10~25 mm. In Figure 8(e) and (g), the curves of K_I on both sides are crossed each other when the crack length is about 10~33mm. As shown in Figure 8(i), K_I at front 1 is higher than that at front 2. Moreover, the slope of K_I curve decreases when the crack is far from the weld. The reason is that the longitudinal residual stress is tensile in the immediate vicinity of the weld and tends to be compressive away from the weld, and the elastic constant increases when cracks enter the base material.

For λ = 0~0.5, the residual stress field leads to lower K_{II} at the initial crack tip, as shown in Figure 8(b) and (d). Once the crack grows, K_{II} quickly decreases to zero. This trend can also be seen in λ = 1~2 cases. Afterwards, there is almost no change in K_{II}, as seen in Fig .8(b). But K_{II} continuously changes in Figure 8(d). For λ = 1~2, the presence of residual stress field leads to higher K_{II} at the initial crack tip, as plotted in Figure 8(f), (h) and (j). As seen in Figure 8(f), the variation of K_{II} occurs when the crack length is about 1.5~10mm and 30~41mm. In Figure 8(h) and (j), K_{II} varies little with the crack growing.

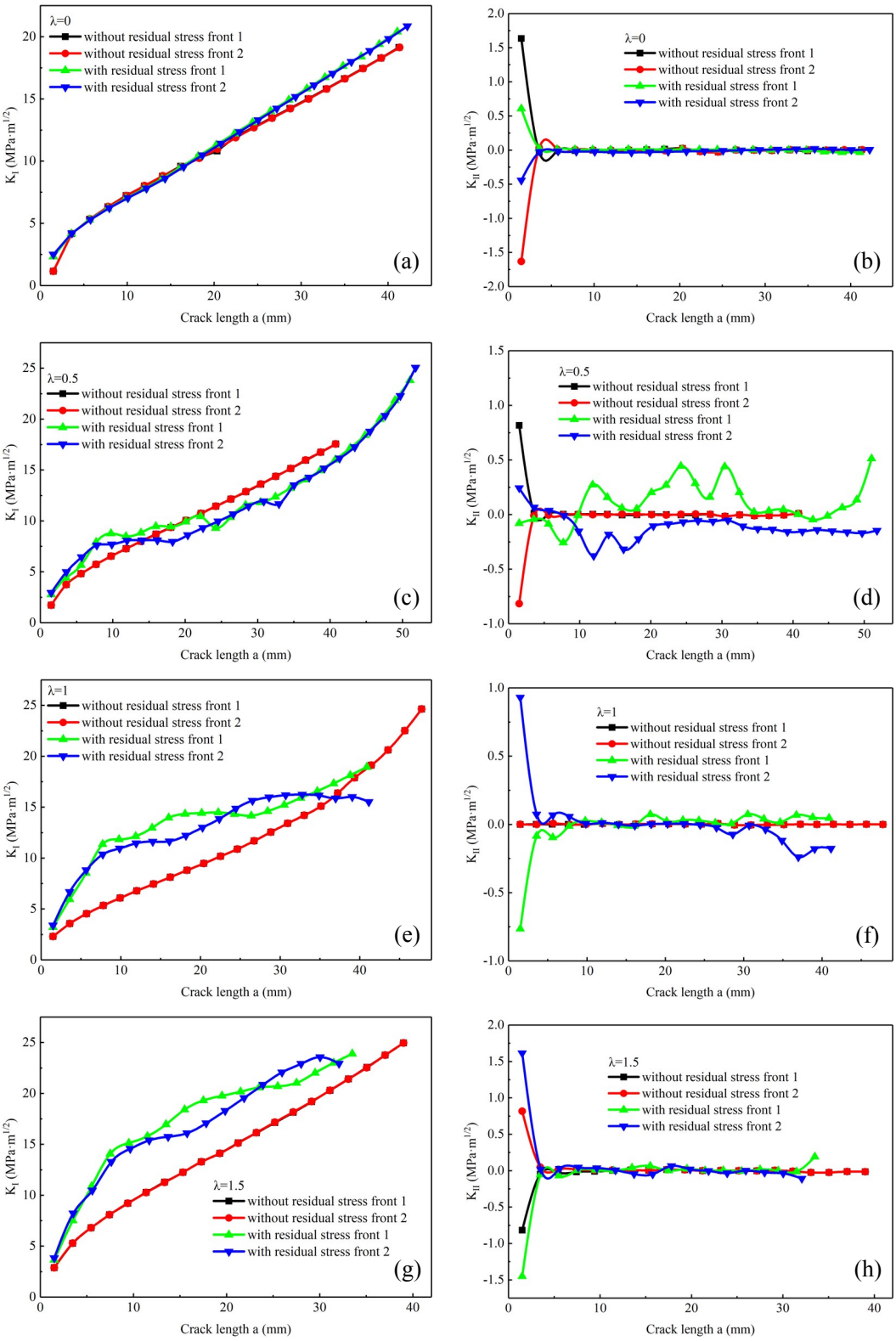
λ=0
without residual stress front 1
without residual stress front 2
with residual stress front 1
with residual stress front 2
K_I (MPa·m^1/2)
K_II (MPa·m^1/2)
Crack length a (mm)
(a)
(b)
λ=0.5
(c)
(d)
λ=1
(e)
(f)
λ=1.5
(g)
(h)

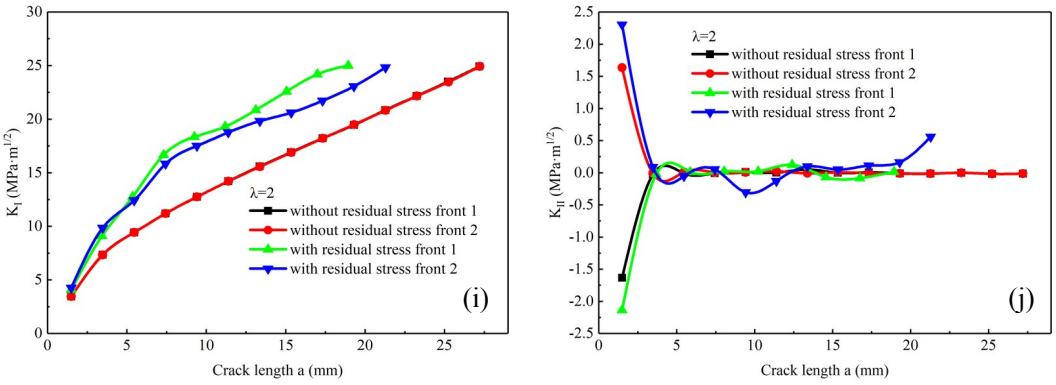

FIGURE 8 SIFs versus crack length

K_I: (a) λ = 0 (c) λ = 0.5 (e) λ = 1 (g) λ = 1.5 (i) λ = 2

K_{II}: (b) λ = 0 (d) λ = 0.5 (f) λ = 1 (h) λ = 1.5 (j) λ = 2

Overall, K_I increases due to the presence of residual stress. K_{II} is mainly affected by residual stress at the beginning of crack propagation. As shown in Figure 8(c)-(j), K_I and K_{II} with residual stress exhibit oscillations apparently, and this indicate that residual stress field has significant effect on the SIFs for λ = 0.5~2. The effects of residual stress on K_I and K_{II} at initial crack tip (a_0 = 1.5) are listed in Table 5.

TABLE 5 Residual stress effects on K_I and K_{II} at initial crack tip (MPa·m$^{1/2}$)

λ	0	0.5	1	1.5	2
K_I-1	1.15↗2.33	1.73↗2.77	2.31↗3.21	2.88↗3.65	3.46↗4.09
K_I-2	1.15↗2.51	1.73↗2.94	2.31↗3.38	2.88↗3.82	3.46↗4.26
K_{II}-1	1.63↘0.61	0.82↘0.08	0↗0.77	0.82↗1.45	1.63↗2.14
K_{II}-2	1.63↘0.44	0.82↘0.24	0↗0.93	0.82↗1.62	1.63↗2.30

5.5 Residual stress intensity factor

In order to investigate the effect of residual stress on the SIFs, the SIF components one related to applied load (K_I^{load} and K_{II}^{load}) and one due to residual stress (K_I^{res} and K_{II}^{res}) has been determined from Eq. (15) and Eq. (16) in Section 5.2. The evolution of SIF components (K_I^{load}, K_{II}^{load}, K_I^{res} and K_{II}^{res}) on both sides for

different biaxial loading ratios is presented in Figure 9. SIFs for all λ cases are listed in Table 6.

Figure 9(a) and (b) show the profile of SIF components at front 1 and front 2 with λ = 0. The SIF components at front 1 is similar to that at front 2. K_I^{load} is increased quickly with crack growing, and K_{II}^{load}, K_I^{res} and K_{II}^{res} are increased slowly. Residual stress has little effect on K_I, so K_I is determined by the applied load. The profile of SIF components at front 1 with λ = 0.5 is displayed in Figure 9(c), unlike those in λ = 0, K_{II}^{load}, K_I^{res} and K_{II}^{res} increased when the crack length is short and then decreased when the crack increases to a certain length. The similar tendency of SIFs at front 2 is shown in Figure 9(d). The highest K_I^{res} is found at about 10mm on both sides, and the maximum K_{II}^{load} and K_{II}^{res} appears at 20~25mm for front 1 side and at 30~35mm for front 2 side respectively. Residual stress has an important effect on K_I, and K_I^{res} is greater than K_I^{load} at about 5~17mm for front 1 and 2~15mm for front 2. The profile of SIF components at front 1 and front 2 with λ = 1 are presented in Figure 9(e) and (f). K_I is residual stress dominated at crack length 5~10mm for front 1 and 2~10mm for front 2. The differences in K_I^{load}, K_{II}^{load} and K_{II}^{res} are not pronounced.

Figure 9(g) and (h) show the profile of SIF components at front 1 and front 2 under λ = 1.5 loading. K_I^{res} is always smaller than K_I^{load}. It means that K_I is applied load dominated with λ = 1.5. When λ = 2, SIF components at front 1 and front 2 plotted in Figure 9(i) and (j) show that K_I is also dominated by the applied load and the residual stress has more effect on K_I at front 2 than that at front 1 in the early stage of crack propagating. K_I^{load}, K_{II}^{load} and K_{II}^{res} are almost the same on both sides. For all cases, K_I^{load} and K_I^{res} is 1.25~24.51 MPa·m$^{1/2}$ and 0.39~5.94 MPa·m$^{1/2}$. K_{II} is composed of K_{II}^{load} and K_{II}^{res}. K_{II}^{load} is -2.68~2.68 MPa·m$^{1/2}$, almost the same as K_{II}^{res}.

The difference in SIF components between front 1 and front 2 is caused by the asymmetric distribution of residual stress field.

Overall, K_I is mainly affected by the applied load. The contribution of residual stress to K_I is related to the biaxial loading ratio. Both K_{II}^{load} and K_{II}^{res} play the important role on K_{II}. The difference between crack propagation paths with and without residual stress for lower biaxial loading ratios (λ = 0~1), as shown in Figure 6(a)-(c), can be attributed to K_{II}^{res}. Therefore, residual stresses contribute to a higher proportion of K_{II} compared to that of K_I.

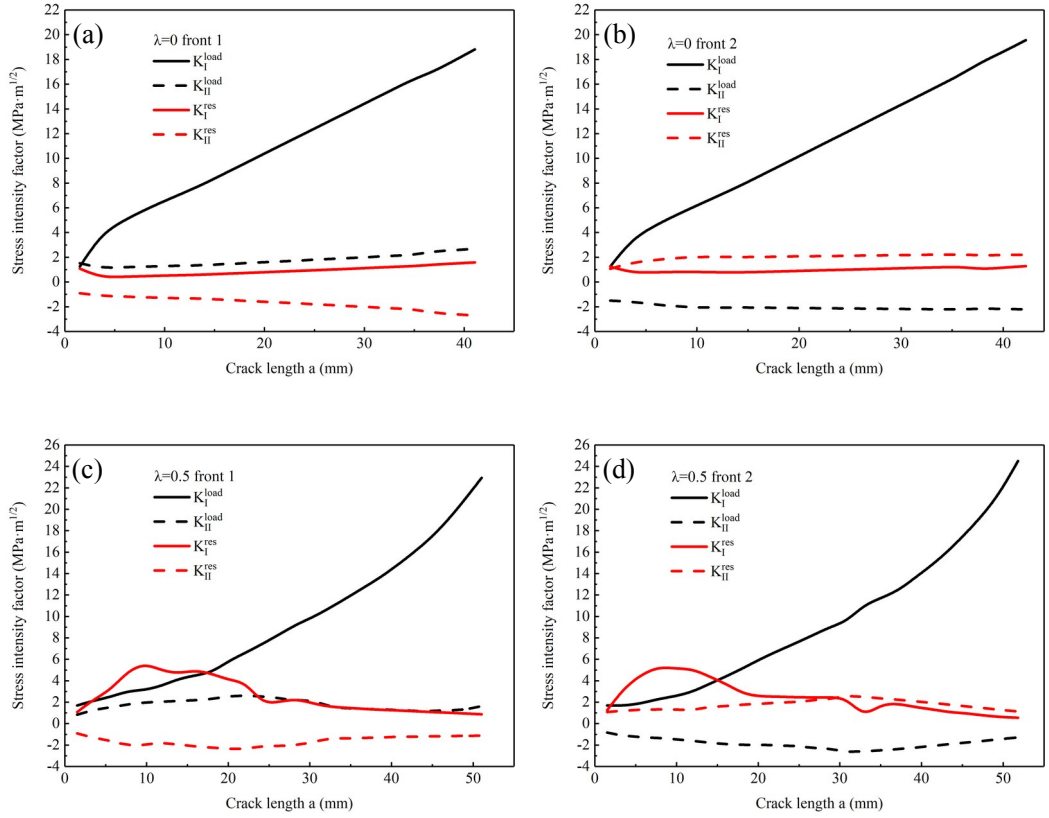

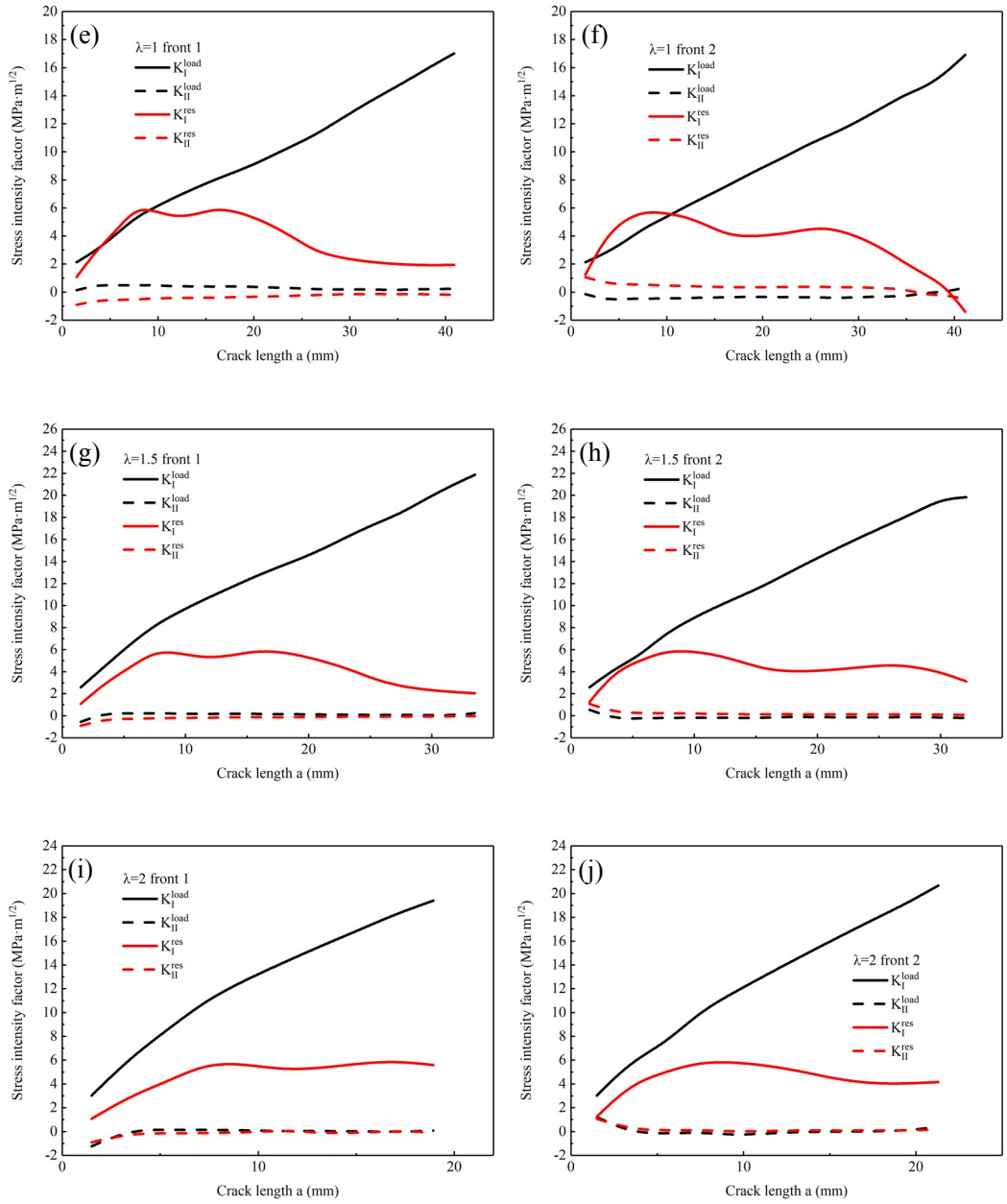

FIGURE 9 SIF components caused by the applied load and residual stress

front 1 (Advancing side): (a) λ = 0 (c) λ = 0.5 (e) λ = 1 (g) λ = 1.5 (i) λ = 2

front 2 (Retreating side): (b) λ = 0 (d) λ = 0.5 (f) λ = 1 (h) λ = 1.5 (j) λ = 2

TABLE 6 SIF components (K_I^{load}, K_{II}^{load}, K_I^{res} and K_{II}^{res}) on both sides for different biaxial loading ratios (MPa·m$^{1/2}$)

λ	0	0.5	1	1.5	2

K_I^{load}-1	1.25~18.82	1.69~22.94	2.13~17.01	2.57~21.86	3.01~19.40
K_I^{load}-2	1.26~19.56	1.68~24.51	2.14~16.91	2.57~19.82	3.01~20.66
K_{II}^{load}-1	1.51~2.68	0.83~2.62	0.14~0.51	-0.54~0.25	-1.23~0.15
K_{II}^{load}-2	-1.51~2.21	-2.68~-0.83	-0.55~0.33	-0.29~0.54	-0.30~1.23
K_I^{res}-1	0.39~1.08	0.88~5.63	1.08~5.94	1.08~5.86	1.08~5.92
K_I^{res}-2	0.75~1.28	0.55~5.29	0.42~5.74	1.25~5.87	1.25~5.84
K_{II}^{res}-1	-2.71~-0.91	-2.37~-0.91	-0.91~-0.14	-0.91~-0.04	-0.91~0.06
K_{II}^{res}-2	1.07~2.23	1.07~2.62	-0.50~1.07	0.08~1.07	-0.01~1.07

The effect of residual stress on SIFs is presented by the ratio of residual SIFs to SIFs plotted against crack length. $K_I^{res} / (K_I^{load} + K_I^{res})$ at λ = 0~2 versus crack length is shown in Figure 10(a). For all cases, an increase of biaxial loading ratio (λ = 0.5~2) leads to decrease of the effect of residual stresses on K_I. $K_I^{res} / (K_I^{load} + K_I^{res})$ reach the maximum values at about 5~10mm, afterwards they are gradually decreased. The direct reason is that residual stresses decreased in the vicinity of weld-edge. On the other hand, this may be attributed to the fact that for short crack the crack is mainly affected by the tensile residual stresses, and it is more influenced from the compressive residual stresses as the crack grows away from the notch.[54]

In Figure 10(b), $K_{II}^{res} / (K_{II}^{load} + K_{II}^{res})$ versus crack length is shown. The maximum $K_{II}^{res} / (K_{II}^{load} + K_{II}^{res})$ increased with increasing biaxial loading ratio (λ = 0.5~2), as it is mainly affected by the residual stress field, especially the transverse residual stress. However, the residual stress effects on crack deviation angle is decreased with increasing biaxial loading ratio. The main reason for this difference is

that the effect of K_{II}^{res} on the variation of crack deviation angle decreased with increasing transverse load, and it also depends on the magnitude of residual stress and the applied load.

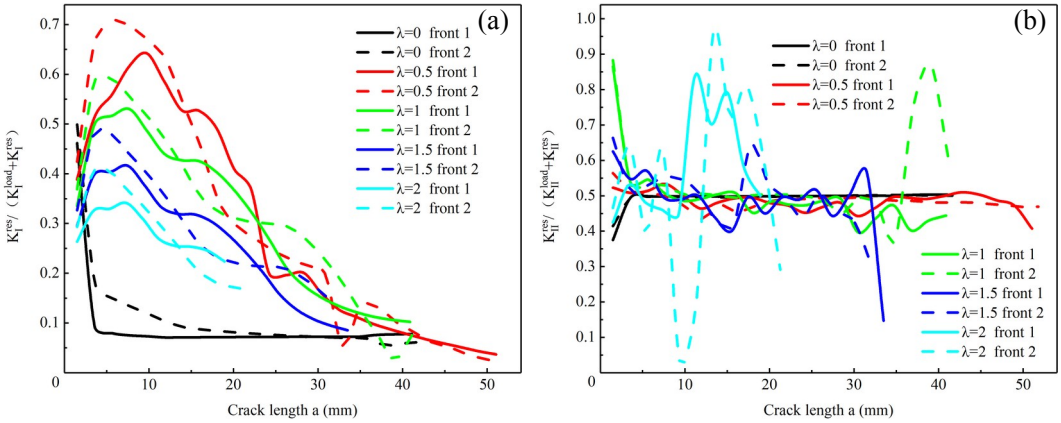

FIGURE 10 Nondimensional (a) $K_I^{res} / (K_I^{load} + K_I^{res})$ and (b) $K_{II}^{res} / (K_{II}^{load} + K_{II}^{res})$ versus crack length for λ = 0~2

For all cases, the residual stress around the crack tips is able to increase SIFs. The maximum $K_I^{res} / (K_I^{load} + K_I^{res})$ and $K_{II}^{res} / (K_{II}^{load} + K_{II}^{res})$ is changing in the range of approx. 33%~70% and 50%~96%. The ratio of residual SIFs to SIFs at front 2 appears higher than that at front 1. This can be explained by the residual stress distributions in the working area, as shown in Figure 3. As a whole, longitudinal and transverse residual stresses in the retreating side are higher than that in the advancing side, although the maximum tensile residual stress is presented in the advancing side. Therefore, we conclude that the effect of residual stresses on K_I and K_{II} in the retreating side is higher than that in the advancing side.

6 CONCLUSION

1. FSW resulted in complex residual stresses in the working area. The longitudinal residual stress exhibited a double-peaked feature with the maximum tensile stress 43.6MPa and the maximum compressive stress -50.2MPa. The transverse residual stress presented a V-shaped distribution with the maximum tensile stress 20.7MPa and the maximum compressive stress -40MPa.

2. Residual stress can change the nominal biaxial loading ratio and affect the crack behaviors. The effect of residual stress on crack deflection mainly appears at the beginning of crack growing under λ = 0, 1, 1.5 and 2. For λ = 0.5, the crack deflection is continuously observed during the crack growing. The residual stress effects on the crack propagation path is more pronounced for lower biaxial loading ratio (λ = 0, 0.5 and 1) than higher ones (λ = 1.5 and 2). This behavior is associated with the increased transverse load.
3. K_I and K_{II} are susceptible to residual stress under biaxial loading conditions (λ = 0.5, 1 ,1.5 and 2). The effect of residual stress on K_I is decreased with increasing biaxial loading ratio, and the trends are contrary to that of K_{II}. K_I is mainly dominated by the applied load. Both K_{II}^{load} and K_{II}^{res} play an important role in crack propagating. Therefore, residual stresses contribute to a higher proportion of K_{II} compared to that of K_I.
4. The effect of residual stress on K_I and K_{II} in the retreating side is higher than that in the advancing side, hence cracks at the retreating side are more affected by the residual stress.

ACKNOWLEDGEMENT

This study was financially supported by the National Natural Science Foundation of China (Grant Nos. 91860128 and 11572250) and the 2018 Innovation Ability Supporting Program of ShaanXi Province (2018KW-028).

REFERENCES

1. Staron P, Koçak M, Williams S. Residual stresses in friction stir welded Al sheets. *Appl Phys A*. 2002;74(1):s1161-s1162.
2. Thomas W, Nicholas ED, Needham JC, Murch MG, Templesmith P, Dawes CJ. Friction stir welding, international patent application no. PCT/GB92/02203 and GB patent application no. 9125978.8. 6 December 1991.
3. Mishra RS, Ma ZY. Friction stir welding and processing. *Mater Sci Eng, R.* 2005;50(1-2):1-78.
4. Biro AL, Chenelle BF, Lados DA. Processing, microstructure, and residual

stress effects on strength and fatigue crack growth properties in friction stir welding: A Review. *Metall Mater Trans B.* 2012;43(6):1622-1637.
5. Bussu G, Irving PE. The role of residual stress and heat affected zone properties on fatigue crack propagation in friction stir welded 2024-T351 aluminium joints. *Int J Fatigue.* 2003;25(1):77-88.
6. Pouget G, Reynolds AP. Residual stress and microstructure effects on fatigue crack growth in AA2050 friction stir welds. *Int J Fatigue.* 2008;30(3):463-472.
7. John R, Jata KV, Sadananda K. Residual stress effects on near-threshold fatigue crack growth in friction stir welds in aerospace alloys. *Int J Fatigue.* 2003;25(9/11):939-948.
8. Pao PS, Gill SJ, Feng CR, Sankaran KK. Corrosion fatigue crack growth in friction stir welded Al 7050. *Scr Mater.* 2001;45(5):605-612.
9. Jata KV, Sankaran KK, Ruschau JJ. Friction stir welding effects on microstructure and fatigue of aluminum alloy 7050-T7451. *Metall Mater Trans A.* 2000;31(9):2181-2192.
10. Ma YE, Liu BQ, Zhao ZQ. Crack paths in a friction stir-welded pad-up for fuselage applications. *J Aircr.* 2013;50(3):879-885.
11. Misak HE, Perel VY, Sabelkin V, Mall S. Crack growth behavior of 7075-T6 under biaxial tension–tension fatigue. *Int J Fatigue.* 2013;55:158-165.
12. Misak HE, Perel VY, Sabelkin V, Mall S. Corrosion fatigue crack growth behavior of 7075-T6 under biaxial tension–tension cyclic loading condition. *Eng Fract Mech.* 2013;106:38-48.
13. Truchon M, Amestoy M, Dang-Van K. Experimental study of fatigue crack growth under biaxial loading, advances in fracture research. 5th International Conference on Fracture; March 29 to April 3, 1981; Cannes, France.
14. Hopper CD, Miller KJ. Fatigue crack propagation in biaxial stress fields. *J Strain Anal Eng Des.* 1977;12(1):23-28.
15. Kibler JJ, Roberts R. The Effect of biaxial stresses on fatigue and fracture. *J Eng Ind Trans ASME.* 1970;92(4):727-734.
16. Lee EU, Taylor RE. Fatigue behavior of aluminum alloys under biaxial loading. *Eng Fract Mech.* 2011;78(8):1555-1564.
17. Zhang X, Zhang H, Bao R. Mode I fatigue crack growth behaviour in a welded cruciform joint under biaxial stresses. 13th International Conference on Fracture; June 16 to 21, 2013; Beijing, China.
18. Richter-Trummer V, Zhang X, Irving PE, Pacchione M, Beltrão M, dos Santos JF. Fatigue crack growth behaviour in friction stir welded aluminium-lithium alloy subjected to biaxial loads. *Exp Tech.* 2016;40(3):921-935.
19. Sutton MA, Reynolds AP, Junhui Yan, Yang B, Yuan N. Microstructure and mixed mode I/II fracture of AA2524-T351 base material and friction stir welds. *Eng Fract Mech.* 2006;73(4):391-407.
20. Smith EW, Pascoe KJ. The behaviour of fatigue cracks subject to applied biaxial stress: a review of experimental evidence. *Fatigue Fract Eng Mater Struct.* 1983;6(3):201-224.

21. Shlyannikov VN, Zakharov AP. Multiaxial crack growth rate under variable T-stress. *Eng Fract Mech.* 2014;123(8):86-99.
22. Fitzpatrick M, Fry A, Holdway P. NPL good practice guide no. 52: determination of residual stresses by X-ray diffraction—Issue 2. *NPL, Great Britain.* 2005.
23. Ma YE, Staron P, Fischer T, Irving PE. Size effects on residual stress and fatigue crack growth in friction stir welded 2195-T8 aluminium – Part I: Experiments. *Int J Fatigue.* 2011;33(11):1417-1425.
24. Prime MB, Gnäupel-Herold T, Baumann JA, Lederich RJ, Bowden DM, Sebring RJ. Residual stress measurements in a thick, dissimilar aluminum alloy friction stir weld. *Acta Mater.* 2006;54(15):4013-4021.
25. Sih G, Paris P, Erdogan F. Crack-tip, stress-intensity factors for plane extension and plate bending problems. *J Appl Mech.* 1962;29(2):306-312.
26. Erdogan F, Sih GC. On the crack extension in plates under plane loading and transverse shear. *J Basic Eng.* 1963;85(4):519-525.
27. Sih GC. Strain energy density factor applied to mixed mode crack problems. *Int J Fract.* 1974;10(3):305-321.
28. Hellen TK, Blackburn WS. The calculation of stress intensity factors for combined tensile and shear loading. *Int J Fract.* 1975;11(4):605-617.
29. Theocaris PS, Kardomateas GA, Andrianopoulos NP. Experimental study of the T-criterion in ductile fractures. *Eng Fract Mech.* 1983;17(5):439-447.
30. Theocaris PS, Andrianopoulos NP. The T-criterion applied to ductile fracture. *Int J Fract.* 1982;20(4):R125-R130.
31. Li C. Vector CTD criterion applied to mixed mode fatigue crack growth. *Fatigue Fract Eng Mater Struct.* 2007;12(1):59-65.
32. Wu X, Li X. Analysis and modification of fracture criteria for mixed-mode crack. *Eng Fract Mech.* 1989;34(1):55-64.
33. Chambers AC, Hyde TH, Webster JJ. Mixed mode fatigue crack growth at 550°c under plane stress conditions in Jethete M152. *Eng Fract Mech.* 1991;39(3):603-619.
34. Gosch A, Berer M, Hutař P, et al. Mixed mode I/III fatigue fracture characterization of Polyoxymethylene. *Int J Fatigue.* 2020;130:105269.
35. Irwin GR. Fracture mechanics in structural mechanics. Proceedings of the 1st Symposium on Naval Structural Mechanics; August 11 to 14, 1958; Stanford University, California.
36. Richard HA, Schramm B, Schirmeisen NH. Cracks on mixed mode loading – Theories, experiments, simulations. *Int J Fatigue.* 2014;62(5):93-103.
37. Reimers P. Simulation of mixed mode fatigue crack growth. *Comput Struct.* 1991;40(2):339-346.
38. Takao O, Machida S, Nakamura T, Tanaka H, Kuwayama K, Asakawa M. Fatigue crack growth of friction-stir-welded aluminum alloy. *J Aircr.* 2016;54:1-10.
39. Sillapasa K, Surapunt S, Miyashita Y, Mutoh Y, Seo N. Tensile and fatigue behavior of SZ, HAZ and BM in friction stir welded joint of rolled 6N01

aluminum alloy plate. *Int J Fatigue.* 2014;63:162-170.
40. http://www.matweb.com/.
41. Wang Q, Zhang W, Jiang S. Fatigue life prediction based on crack closure and equivalent initial flaw size. *Materials.* 2015;8(10):7145-7160.
42. Ma YE, Staron P, Fischer T, Irving PE. Size effects on residual stress and fatigue crack growth in friction stir welded 2195-T8 aluminium – Part II: Modelling. *Int J Fatigue.* 2011;33(11):1426-1434.
43. Gadallah R, Osawa N, Tanaka S, Tsutsumi S. A novel approach to evaluate mixed-mode SIFs for a through-thickness crack in a welding residual stress field using an effective welding simulation method. *Eng Fract Mech.* 2018;197(Jun.15):48-65.
44. Kc A, Kim J-H. Interaction integrals for thermal fracture of functionally graded materials. *Eng Fract Mech.* 2008;75(8):2542-2565.
45. Ayatollahi MR, Saboori B. A new fixture for fracture tests under mixed mode I/III loading. *Eur J Mech A Solids.* 2015;51:67-76.
46. Rice J. A path integral and the approximate analysis of strain concentration by notches and cracks. *J Appl Mech.* 1968;35(2):379-386.
47. Kim J-H, Paulino GH. The interaction integral for fracture of orthotropic functionally graded materials: evaluation of stress intensity factors. *Int J Solids Struct.* 2003;40(15):3967-4001.
48. Anderson T. *Fracture Mechanics – Fundamentals and Applications.* Vol 1, 1991.
49. Liu H. *Fatigue crack behaviors under biaxial loading*, MD thesis. Northwestern Polytechnical University; 2017.
50. Neerukatti RK, Datta S, Chattopadhyay A, Iyyer N, Phan N. Fatigue crack propagation under in-phase and out-of-phase biaxial loading. *Fatigue Fract Eng Mater Struct.* 2018;41(2):387-399.
51. Perel VY, Misak HE, Mall S, Jain VK. Biaxial fatigue crack growth behavior in aluminum alloy 5083-H116 under ambient laboratory and saltwater environments. *J Mater Eng Perform.* 2015;24(4):1565-1572.
52. Rubinstein AA. Mechanics of the crack path formation. *Int J Fract.* 1991;47(4):291-305.
53. Seitl S, Knésl Z. Two parameter fracture mechanics: Fatigue crack behavior under mixed mode conditions. *Eng Fract Mech.* 2008;75(3-4):857-865.
54. Labeas G, Diamantakos I. Numerical investigation of through crack behaviour under welding residual stresses. *Eng Fract Mech.* 2009;76(11):1691-1702.